

# Observation of Soliton Molecules in a Robust All PM Mode-Locked Fiber Laser With Nonreciprocal Phase Bias

Volume 13, Number 1, February 2021

Renlai Zhou, *Member, IEEE*

Xuanyi Liu

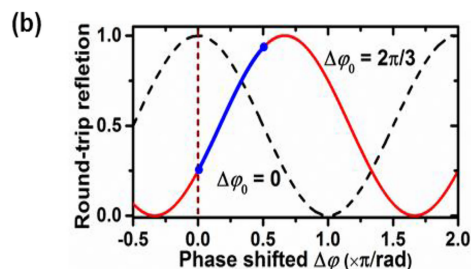
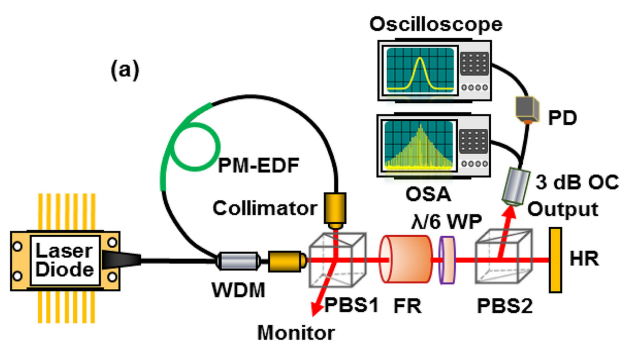
M S Aruna Gandhi, *Member, IEEE*

Guanyu Liu

H. Y. Fu, *Member, IEEE*




Zhigang Zhang

Qian Li, *Member, IEEE*



DOI: 10.1109/JPHOT.2020.3043425

# Observation of Soliton Molecules in a Robust All PM Mode-Locked Fiber Laser With Nonreciprocal Phase Bias

Renlai Zhou <sup>1</sup>, Member, IEEE, Xuanyi Liu,<sup>1</sup>  
M S Aruna Gandhi,<sup>1</sup> Member, IEEE, Guanyu Liu,<sup>2</sup>  
H. Y. Fu <sup>3</sup>, Member, IEEE, Zhigang Zhang,<sup>4</sup>  
and Qian Li <sup>1</sup>, Member, IEEE

<sup>1</sup>School of Electronic and Computer Engineering, Peking University,  
Shenzhen 518055, China

<sup>2</sup>Guangdong Provincial Key Laboratory of Optical Fiber Sensing and Communications,  
Institute of Photonics Technology, Jinan University, Guangzhou 510632, China

<sup>3</sup>Tsinghua-Berkeley Shenzhen Institute (TBSI), Tsinghua University,  
Shenzhen 518055, China

<sup>4</sup>State Key Laboratory of Advanced Optical Communication Systems and Networks, School  
of Electronics Engineering and Computer Science, Peking University, Beijing 100871, China

DOI:10.1109/JPHOT.2020.3043425

This work is licensed under a Creative Commons Attribution 4.0 License. For more information, see  
<https://creativecommons.org/licenses/by/4.0/>

Manuscript received September 17, 2020; revised December 4, 2020; accepted December 4, 2020.  
Date of publication December 9, 2020; date of current version January 6, 2021. This work was  
supported in part by the National Natural Science Foundation of China (61805281, 61675008); in  
part by Natural Science Foundation of Guangdong Province, China (2019A1515010732); and in part  
by Tsinghua-Berkeley Shenzhen Institute (TBSI) Faculty Start-up Fund and Shenzhen Technology  
and Innovation Council (Project: JCYJ20180507183815699). Corresponding author: Qian Li (e-mail:  
liqian@pkusz.edu.cn).

**Abstract:** We report the first experimental observation, to the best of our knowledge, of soliton molecules in a robust all polarization-maintaining (PM) mode-locked fiber laser with a nonreciprocal phase bias that results in a low self-starting threshold and stable mode locking. Through elaborately tuning the waveplate in the cavity, calibrating the laser pulse from conventional soliton to soliton molecules is implemented, and versatile soliton molecules including harmonic soliton pairs, tightly or loosely bound soliton quartets, multi-pulse bound solitons are achieved and manipulated at different pump powers. Theoretical investigations are established to elucidate the soliton molecules spectral characteristics with various phase differences and time separations in the cavity that elicit good concurrence with achieved experimental results. The achieved results both rich the nonlinear dynamics in fiber lasers and pave the potential applications for this excellent architecture fiber laser.

**Index Terms:** Soliton molecules, mode-locking, fiber laser.

## 1. Introduction

As a hot research focus, soliton molecules (SMs) have attracted great interest over the past few years, that illuminate to comprehend the interaction mechanism among the soliton pulses in the cavity, and have potential applications in the fields of optical information storage [1], optical telecommunication systems with high capacity [2], and optical signal processing [3]. Thanks to the first theoretical prediction of SMs by the models of the coupled Ginzburg-Landau equation and non-linear Schrödinger equation in fiber lasers [4]. Heretofore, various SMs have been experimentally

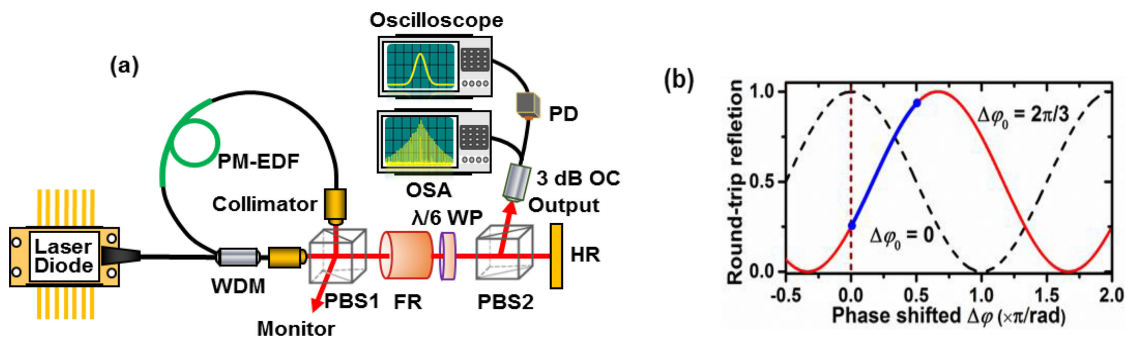


Fig. 1. Schematic of the mode-locking fiber laser configuration with a biased NALM: (a) experimental setup, (b) round-trip transmission curve with a  $2\pi/3$  nonreciprocal phase bias (red solid curve) and no phase bias (black dashed curve).

exemplified in soliton [5], stretched-pulse [6], self-similar [7], and gain-guided [8], spatiotemporal mode-locking [9], and nonlinear multimode interference effect [10]. According to the operation conditions, the soliton interactions in SMs formation mayhap categorized into three types [11]: direct, localized, and global soliton-soliton interactions. Three different perturbations of third-order dispersion (dispersive wave generation), the periodic nature of the cavity (Kelly sidebands), and the random birefringence of the resonator were experimentally evidenced during the bound state formation in a ring fiber laser [9]. Generally, the aforementioned soliton interactions can coexist in the cavity, therefore numerous interesting SMs mayhap formed by complex soliton-soliton interactions in fiber lasers.

Recently, all PM nonlinear amplifying loop mirror (NALM) mode-locking fiber lasers with various nonreciprocal phase biases are of great interest [13]–[16]. Compared with the mode-locking techniques of real SAs, NPR, and NOLM, potential advantages are discribed in this type all PM fiber laser, such as good self-starting ability, excellent environmental stability, and lower intrinsic noise. W. Hänsel et al. [14] demonstrated a novel architecture of fiber laser with nonreciprocal phase bias, that mayhap used to generate femtosecond pulses with different wavelengths. Up to 700 MHz fundamental repetition rate self-starting  $\text{Yb}^{3+}$ -doped fiber laser with a phase biased NALM was demonstrated [15], that facilitates good environmental stability and lower intensity/phase noise. A 44.6 fs mode-locked non-PM  $\text{Er}^{3+}$ -doped fiber (EDF) laser have been reported by W. Gao et al. [16], employed the shortest pulse duration. However, only the basic output characteristics of mode-locking laser are reported in this architecture, the fascinating nonlinear phenomenon of SMs, harmonics mode-locking (HML) is not observed.

In this letter, to the best of our knowledge, we report the first experimental observation of various SMs in an all PM mode-locked fiber laser based on a phase biased NALM. By finely adjusting the waveplate inside the cavity, manipulation of the laser pulses from conventional soliton to various SMs has been realized. Output characteristics of multiple SMs are measured and compared under different operation conditions in detail. Moreover, the spectral characteristics of soliton molecules with various phase differences and time separations are theoretically analyzed, and the calculative results are consistent with the experiment.

## 2. Experimental Setup and Operation Principle

The experimental schematic of the mode-locked fiber laser is shown in Fig. 1(a). A 976 nm pump laser is launched into a high-gain 0.8 m PM-EDF (PM-ESF-7/125, Nufern) through a PM fiber 980/1550 nm wavelength-division multiplexer (WDM), that can simultaneously work in fast and slow axis, and the absorption coefficient of gain fiber is 24 dB/m. In order to improve the stability and coupling efficiency, two fiber collimators and a polarizing beam splitter (PBS) are integrated as a device. As the key part of mode-locking laser, a  $\lambda/6$  waveplate and a Faraday rotator (FR) are

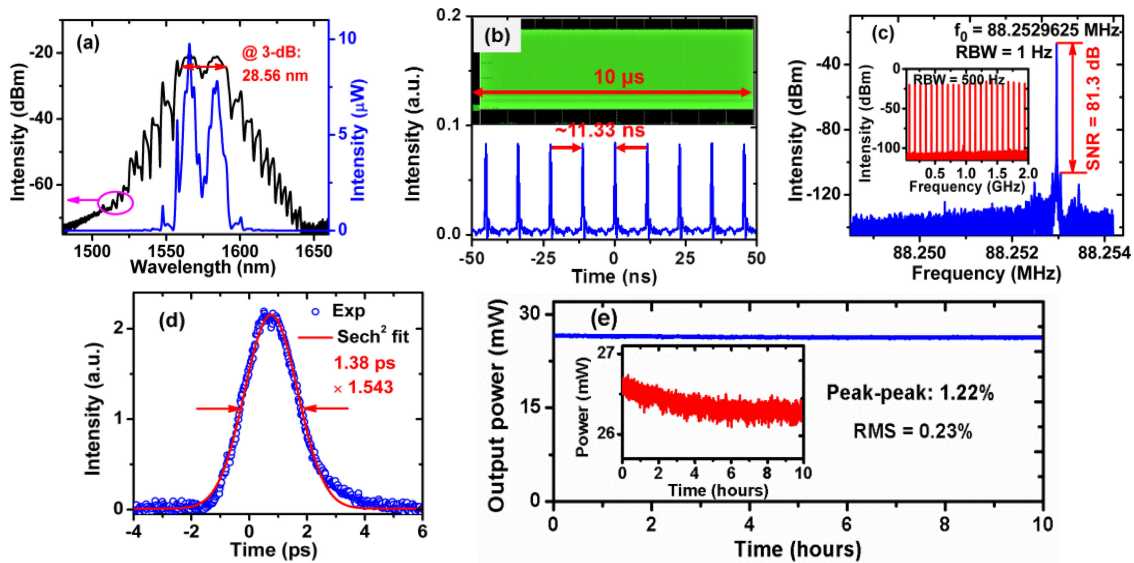


Fig. 2. The output characteristics of the mode-locking fiber laser: (a) output optical spectra; (b) output pulses train; (c) RF spectra; (d) intensity AC trace; and (e) stability of output power at 26.4 mW.

combined together which serves the non-reciprocal phase bias of  $2\pi/3$  in the roundtrip. An optical spectrum analyzer (OSA, AQ6370D, Yokogawa) with a tunable resolution of 0.02 to 2 nm is used for spectrum measurement. A radio frequency (RF) signal analyzer (N9030B, Agilent) with a bandwidth of 3 Hz - 50 GHz is used to monitor the RF spectrum of laser pulses. A  $>25$  GHz bandwidth InGaAs photodiode detector (PD, UPD-15-IR2-FC) and a real-time 20 GHz sampling oscilloscope (DSO-X 6004A, Keysight) are employed to detect the pulse train. A power meter (S148C, Thorlabs) with a power range from 1  $\mu$ W to 1 W is used to measure the output power and monitor the power stability. A commercial autocorrelator (FR-103XL, Femtochrome) is used to analyze the intensity AC traces of soliton pulses.

The roundtrip transmission of NALM with a nonreciprocal phase bias is indicated in Fig. 1(b).  $\Delta\varphi_0$  is the original phase of NALM, and  $\Delta\varphi$  is the nonlinear phase shift in the cavity. Without any phase bias (black dash curve), the reflectivity function has the highest value at  $\Delta\varphi = 0$ , whereas it shows a vanishing slope. By offering a  $2\pi/3$  phase bias, the reflectivity curve shifts to the right and this allows the fiber laser to work at positive feedback reflection region, which corresponds to the nonlinear phase shift from 0 to  $\pi/2$  as depicted in Fig. 1(b). The  $2\pi/3$  non-reciprocal phase bias releases the requirement of extra nonlinear phase shift, as a result, the self-starting ability of mode-locking is enhanced. Our previous results showed that the self-starting threshold of mode-locking is relevant to the slope of reflectivity curve, where a steeper reflectivity slope is beneficial to the mode-locking operation [17].

### 3. Results and Discussion

As a result of the inserted  $2\pi/3$  phase bias in the cavity the mode-locking operation is directly built up at pump power of 430 mW. Eventually, decreasing the pump power to 350 mW, the stable single pulse soliton is achieved and the measured output power is 26.4 mW. Figure 2(a) depicts the measured output spectrum produced by the mode-locked fiber laser. Obvious sidebands are seen in the spectrum, and the 3-dB spectral bandwidth is 28.56 nm. It is evident that two central wavelengths are clearly distinguished in the spectrum which is caused by the coherent interference between the two combined beams. Several CW lasers with the wavelengths of 1565.688, 1557.476 and 1547.721 nm are visible in the spectrum. The oscilloscope trace of the pulse train is monitored, and shown in Fig. 2(b). It is conspicuous that the pulses train is stable, and the interval of the

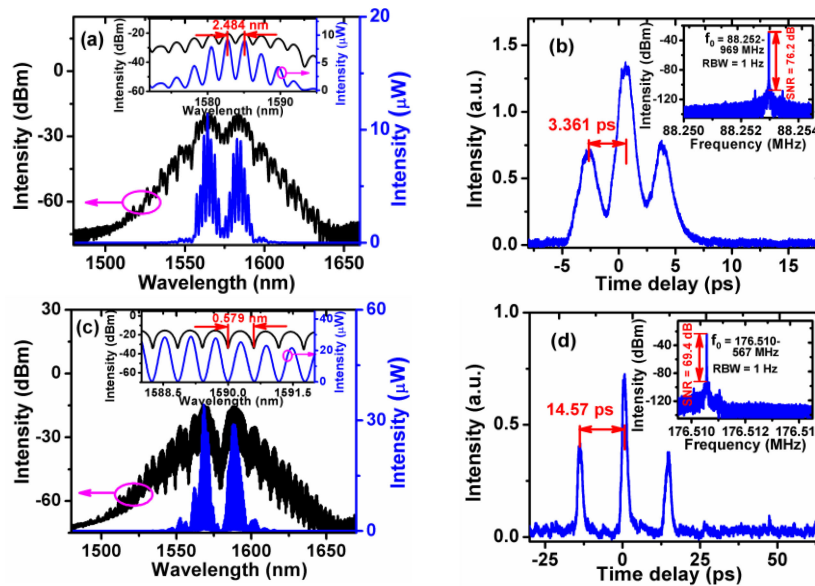


Fig. 3. Experiment results of the bound soliton pairs: (a), (b) the optical spectra and intensity AC trace of fundamental soliton pairs; (c), (d) the optical spectra and intensity AC trace of harmonic soliton pairs.

adjacent pulses is about 11.33 ns, which is consistent with the cavity roundtrip time. The screenshot of the pulse train with 10  $\mu$ s time range is shown in the inset of Fig. 2(b). The profile of temporal pulse is constant and stable, and no perturbation is noticed. The RF spectrum distribution is presented in Fig. 2(c) with a resolution bandwidth (RBW) of 1 Hz and a span of 5.7 kHz. The pulse repetition rate is 88.2529625 MHz, which is in accordance with the fundamental repetition rate of the cavity. The signal-to-noise ratio (SNR) is over 81 dB, indicating the mode-locking operation is stable regime. A 2 GHz wideband RF spectrum is presented in the inset of Fig. 2(c), and no envelope modulation is found. The fine structure of the laser pulse is measured, and illustrated in Fig. 2(d). The full width at half maximum (FWHM) of the pulse duration is about 1.38 ps, calculated by fitting the sech<sup>2</sup> profile to the pulse. The time-bandwidth product (TBP) is calculated to be 4.76, suggesting the pulse is strongly chirped. To assess the long-term stability of mode-locking operation of this all PM fiber laser, the average output power at 26.4 mW is monitored in the open air at room temperature. As demonstrated in Fig. 2(e), the power fluctuations are approximately 0.48% root mean square (RMS) and 1.22% peak-peak fluctuation when the laser is continuously running around 10 hours. The breakup of the mode locking is not observed, that results in a dramatic shaking in the output power. The zoomed-in power fluctuation is shown in the inset of Fig. 2(e). It can be found that the output power gradually decreases, and reaches a stable 26.4 mW after about 6 hours.

Solitons formation in anomalous dispersion regime results from the balance of dispersion and nonlinear effects in the cavity. If the intracavity parameters are varied, the balance of soliton state is broken, and the bound state operation mayhap achieved by the complex soliton-soliton interactions. In the experiment, we finely adjusted the orientation of  $\lambda/6$  waveplate at a pump power of 350 mW, and the stable soliton pair molecule is observed. Figure 3(a) shows measured output spectrum with periodic modulation, which is a typical signature of bound state interference with phase locking. The evident modulated spectrum results from the interference fringes of two closely spaced solitons. The zoomed-in modulated spectrum is inserted in Fig. 3(a), where the revealed modulated period is  $\Delta\nu = \Delta\lambda_c/\lambda_{02} = 297.477$  GHz, for  $\Delta\lambda = 2.484$  nm at  $\lambda_0 = 1582.74$  nm. The corresponding intensity AC trace is depicted in Fig. 3(b), with  $\Delta\tau = 3.361$  ps time separation between two close solitons pulses, being consistent with spectrum modulated period ( $\Delta\nu = 1/\Delta\tau$ ) in Fig. 3(a). It is eminent that the time separation of the adjacent soliton pulses is less than three times of

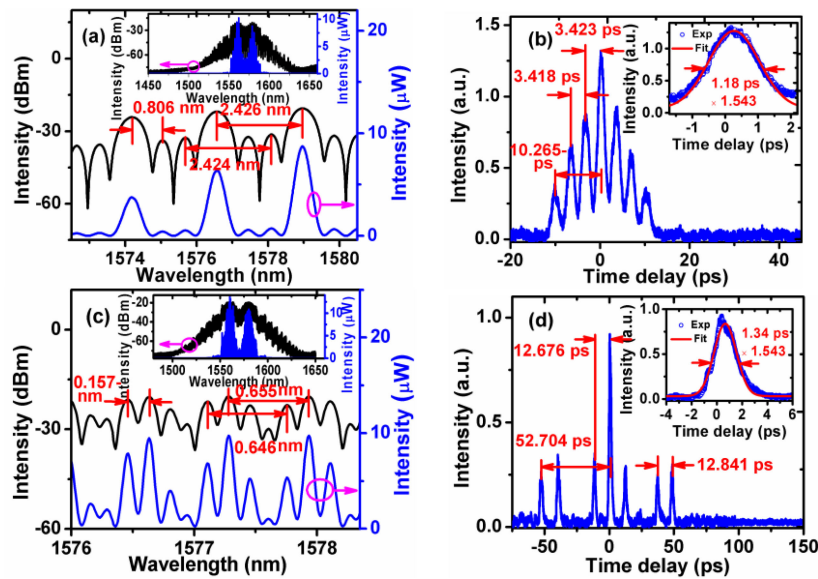


Fig. 4. Soliton quartets under different time separations: (a), (c) are the modulated spectra in enlarged scale and overall spectra; (b), (d) are the intensity AC traces and pulse durations with the  $\text{sech}^2$  fitting.

soliton duration ( $\sim 1.34$  ps), where the direct soliton-soliton interaction force is particularly strong under this condition, and the tightly bound state is formed [11]. The observed intensity ratio of the bound solitons is 1:2:1 that means the two soliton pulses have nearly the same intensity, identical separation, and pulse duration. The pulse repetition rate is 88.252969 MHz with a 1 Hz RBW, shown in inset of Fig. 3(b), and the SNR is over 76 dB, confirming the good stability of the soliton pairs operation. By adjusting the orientation of  $\lambda/6$  waveplate, the modulation depth of the roundtrip reflectivity curve of NALM is regulated, and the transformation of different soliton bound states may be easily achieved. HML operation of the soliton pairs is achieved by further finely rotating the  $\lambda/6$  waveplate. However, if the rotation of the waveplate exceeds a certain range, the mode-locking operation will be lost abruptly. Figure 3(c) shows the measured output spectrum characterized by apparent spectrum interference fringes, and the modulation period is 0.579 nm. Nearly 100% modulation depth implies the two soliton pulses have excellent coherence. The corresponding intensity AC trace is exhibited in Fig. 3(d). Time separation of the adjacent pulses is 14.57 ps, which agrees well with the theoretical value calculated from the 0.579 nm modulation period. The ratio between the time separation and the pulse duration is larger than the setting criterion of direct soliton-soliton interactions, and it belongs to loosely bound state [8]. Under this condition, the direct interaction force between soliton pulses becomes weak, and the long-range interaction force plays the main role in the formation of bound-state pulses. The monitored RF spectrum is illustrated in the inset of Fig. 3(d), the pulse repetition rate is 176.510567 MHz which is about twice the fundamental repetition rate. Over 69 dB SNR indicates high stability of second-order HML in this all PM fiber laser.

As mentioned above, bound states result from the complex soliton-soliton interactions in the cavity, hence the soliton molecules formation are vulnerable to the variation of cavity parameters, viz gain, loss, nonlinearity, and dispersion. When the pump power is increased to 450 mW, the SMs bound with four soliton pulses are achieved in fiber laser. Figure 4(a) (State 1) parades the detailed output spectrum of soliton quartets. Different from the spectra of soliton pairs, noticeable secondary modulation can be observed in the optical spectrum. The measured average spectrum modulation periods are about 2.426, 2.424, and 0.806 nm, respectively, corresponding to the time separations of 3.421, 3.424, and 10.262 ps in theory. From the intensity AC trace in Fig. 4(b), the measured time separations are consistent with the theoretical values calculated from spectrum modulation

TABLE 1  
Detailed Output Characteristics of the Four Types Soliton Quartets

BS	$P_{\text{out}}$ (mW)	$P_{\text{th}}$ (mW)	$t_p$ (ps)	$\kappa_{ir}$
State1	34.2	550	1.18	1:2:3:4:3:2:1
State2	29.2	--	1.34	1:1:1:3.1:1:1:1
State3	31.7	700	1.32	1:1:1:2.7:1:1:1
State4	37.5	430	1.24	1:1:1:3.4:1:1:1

a BS: bound state;  $P_{\text{out}}$ : average output power;  $P_{\text{th}}$ : mode-locking threshold of self-starting;  $t_p$ : pulse duration;  $\kappa_{ir}$ : intensity ratio of different peaks in AC trace.

periods. It can be noted that the intensity ratio of the different peaks in the AC trace is nearly 1:2:3:4:3:2:1, suggesting the bound soliton pulses have almost identical intensities. Different soliton quartets can be achieved by adjusting the waveplate. As demonstrated in Fig. 4(c) (State 2), the spectrum modulation periods of 0.655, 0.646 and 0.157 nm corresponding to the time separations of 12.676, 12.84 and 52.704 ps as shown in Fig. 4(d). The intensity ratio of the different peaks in the AC trace is nearly 1:1:1:3.1:1:1:1, that perhaps caused by the intensity differences of the soliton pulses inside the SM.

With further appropriately adjusting of the waveplate in the cavity, another two types soliton quartets with different modulation periods can also be realized (defined as State 3, 4). Table 1 lays out a more detailed description of the output characteristics of the four types soliton quartets. The average output power is dissimilar under different state, and the maximum output power is 37.5 mW in State 4, and the minimum output power is 29.2 mW in State 2. It is conspicuous that the self-starting threshold is reversely related to the average output power, and the lowest self-starting threshold is 430 mW. For the State 2, the mode-locking cannot be self-started by the limited pump power. The pulse duration is regulated from 1.18 ps to 1.34 ps. More interesting, when the mode-locking operation is experimentally built up, then adjusting the pump power to 450 mW, and the similar SMs are realized anon by appropriately rotating the  $\lambda/6$  waveplate.

Increasing the pump power to 540 mW, a five-soliton pulse SM is achieved. As shown in Fig. 5(a), a series of modulated peaks between adjacent maximum peaks indicates that the complicated interactions amid the inner soliton pulses. The measured spectrum modulation periods are 0.665, 0.653, 0.655, and 0.164 nm which correspond to the time separations of 12.652, 12.694, 12.654, and 50.57 ps in measured intensity AC trace, as shown in Fig. 5(b). The intensity ratio of different peaks in intensity AC trace is nearly 1:1:1.5:1.9:3.6:1.9:1.5:1:1, which implies the unequal intensity of the pulses inside the SM. Further rotating the  $\lambda/6$  waveplate, the multipulse bound solitons are experimentally observed. Figure 5(c) shows the output spectrum of multipulse bound solitons, and the intensity AC trace is present in Fig. 5(d). The spectrum modulation periods of 1.463, 1.463, and 0.154 nm correspond to the time separations of 5.677, 5.678, and 53.81 ps. It can also be noted that the intensity AC trace is composed by three bound state units, one unit is a three-pulse bound state and the other two units are two-pulse bound states. However, this state is unstable, and the pulse intensities and time separations are variable.

From the achieved experimental results, the formation of SMs in the proposed all PM fiber laser can be explicated by the following perspectives. Firstly, a short segment of high-gain PM EDF is used as the gain media, that is more beneficial to the generation of SMs with a fundamental repetition rate [18]. Additionally, the strong birefringence in the laser cavity is more favorable for the formation of SMs [12], [19]. In our experiment, rotating the  $\lambda/6$  waveplate can effectively adjust the intensities in p and s directions of the PBS2, the phase correlations among soliton pulses would be transformed, and the modulation depth of the roundtrip reflectivity curve of NALM is also regulated, leading to versatile bound states formation in the cavity. Moreover, for all the formation of multipulse bound solitons is more complex, it is clear that the bound state formation in each unit

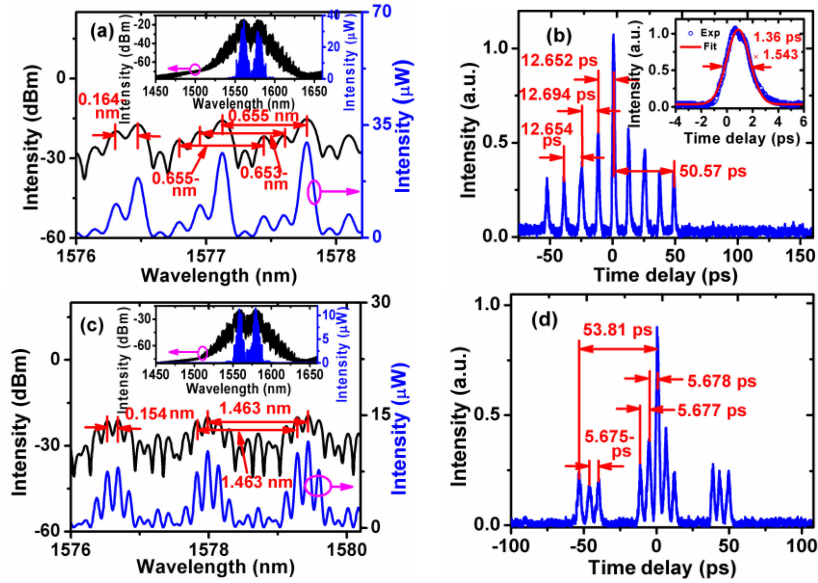


Fig. 5. Multipulse bound solitons with different time separations: (a), (c) are the modulated spectra in enlarged scale and overall spectra; (b), (d) are the intensity AC traces and the pulse duration with the sech2 fitting.

results from the three types of soliton-soliton interactions [20]. For example, the pulse separations in Fig. 5(b) are more than five times of the measured pulse duration, and the long-range soliton-soliton interactions opt in bound state formation. For Fig. 5(d), the adjacent pulse separations are less than five times of the measured pulse duration, signifying the direct soliton-soliton interactions result in the bound state formation.

#### 4. Theoretical Investigation for the Spectrum Characteristics of SM

In consideration of the comprehensive manipulation of the soliton molecules by rotating the waveplate in the cavity, phase difference and time separation between the soliton pulses are the two key components which play essential roles in soliton molecules formation. Here, theoretical investigations are conducted to elucidate the effects of phase difference and time separation on the spectrum modulation, which can further validate the spectral characteristics of the soliton molecules in the experiment.

Assume that the soliton pulses have identical pulse shape and amplitude in molecules. The slowly varying electric field profile of single soliton pulse is  $E_0(t)$  in the time domain.  $\tau_j (j = 1, 2, 3)$  and  $\varphi_j (j = 1, 2, 3)$  are the time separation and phase difference of soliton pulses in molecules. The bound states of soliton pairs and soliton quartets can be described as follow [21]:

$$E_{SP}(t) = E_0(t) + E_0(t + \tau_1) \cdot e^{-i\varphi_1}. \quad (1)$$

$$E_{SQ}(t) = E_0(t) + E_0(t + \tau_1) \cdot e^{-i\varphi_1} + E_0(t + \tau_2) \cdot e^{-i\varphi_2} + E_0(t + \tau_3) \cdot e^{-i\varphi_3}. \quad (2)$$

where SP: soliton pairs, SQ: soliton quartets.

According to the Fourier transform, the corresponding spectrum intensities of soliton pairs and soliton quartets are exemplified in the frequency domain:

$$I_{SP}(\omega) = 2I_0(\omega)[1 + \cos(\omega\tau - \varphi)]. \quad (3)$$

$$I_{SQ}(\omega) = I_0(\omega) \left| 1 + e^{-i(\omega\tau_1 - \varphi_1)} + e^{-i(\omega\tau_2 - \varphi_2)} + e^{-i(\omega\tau_3 - \varphi_3)} \right|^2. \quad (4)$$



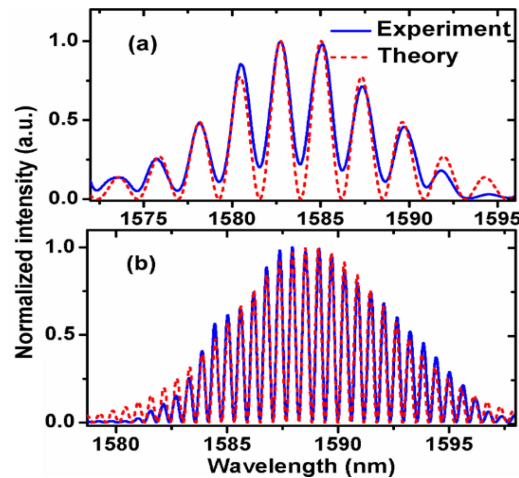


Fig. 6. Theoretical spectrum characteristics of soliton pairs with  $\pi$  phase difference: (a) normalized theoretical spectrum of the tightly bound soliton pairs (red dashed curve) and the experimental result (blue solid curve), the central wavelength is 1583.87 nm; (b) normalized theoretical spectrum of the loosely bound soliton pairs and experimental result, the central wavelength is 1588.82 nm.

where  $\omega$  denotes the angular frequency difference compared to the central optical frequency in the spectrum.  $i = \sqrt{-1}$  is imaginary unit.  $I_0(\omega) = |E_0(\omega)|^2$  is the spectrum intensity profile of the soliton pulse. From above equations, it is apparent the spectrum modulation period is  $\Delta\omega_j = 2\pi/\tau_j$  ( $j = 1, 2, 3$ ), that indicate the spectrum modulation periods in the frequency domain correspond to the time separations in the time domain.

Firstly, the theoretical investigation is implemented to investigate the spectral characteristics of the soliton pairs. The soliton is assumed to be a chirp-free sech pulse shape with different central wavelengths. The pulse separation and pulse duration are consistent with experimental results. The phase difference is set as  $\pi$ . Figure 6(a) shows the normalized theoretical spectrum of the tightly bound soliton pairs. It is noticeable that the numerical result agrees well with the experimental result, and the wavelength peaks of the two spectra are nearly coincident with each other. Compared with the theoretical result, the modulation depth of the measured spectrum is lower than 100%, but the high ratio modulation depth still indicates an excellent coherence of two bound solitons. The theoretical spectrum of loosely soliton pairs is present in Fig. 6(b). The numerical result almost overlaps with the experimental spectrum, and the  $\sim 100\%$  modulation depth suggests highly coherence of two soliton pulses.

Subsequently, theoretical investigation is performed to demonstrate the spectral characteristics of the soliton molecule with four soliton pulses. For the four-pulse bound state, the phase relations between soliton pulses cannot be directly ascertained from the modulation spectrum, and needs to take consideration of the spectrum profile and detailed modulated spectrum. According to the measured output spectra and intensity AC traces, the central wavelengths, time separations, and pulse durations are utilized in calculation. Through elaborately adjusting the phase relations between the soliton pulses, the numerical spectra are present in Figs. 7(a)–(d). The numerical results agree well with the experimental results, which are further manifested by the zoomed-in spectra on the right side, corresponding to the dashed regions in spectra. However, some palpable disagreements between numerical and experimental results are found on the edges of the modulation spectra, and the reasons are examined as follow. Firstly, the assumption of sech-shaped pulses in the calculation is not exactly accurate, that results in inconsistency between the theory and the experiment. Meanwhile, the sidebands generation in the output spectrum can influence the profile of the modulation spectrum. In addition, the asymmetry of gain spectrum of EDF can cause the distortion of modulation spectrum, that in turn to the disagreements.

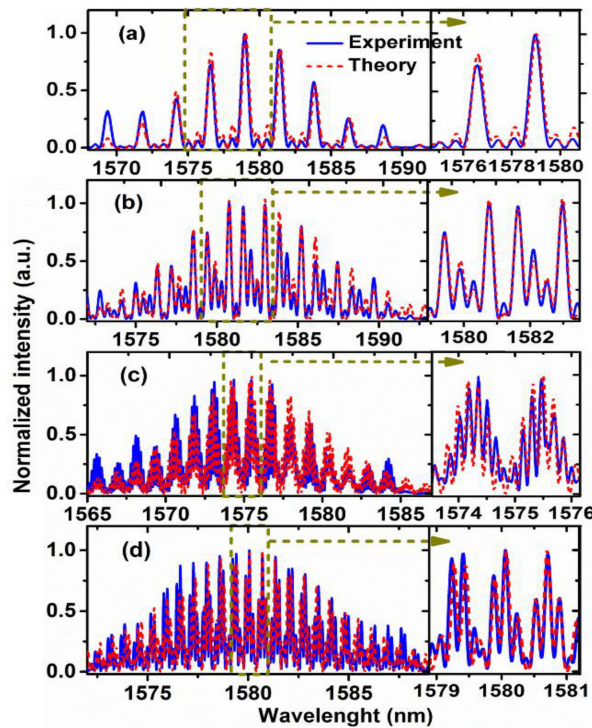


Fig. 7. Theoretical spectrum characteristics of soliton quartets: (a) theoretical spectrum with phase differences of  $\pi/2$ ,  $\pi/2$ , and  $\pi/2$  (red dashed curve) and experimental result (blue solid curve), the central wavelength is 1579.2 nm; (b) theoretical spectrum with phase differences of  $\pi/2$ ,  $\pi$ , and  $\pi/2$ , the central wavelength is 1582.21 nm; (c) theoretical spectrum with phase differences of 0, 0, and  $-\pi/2$ ; and experimental result, the central wavelength is 1575.47 nm; and (d) theoretical numerical spectrum with phase differences of 0, 0, and  $-\pi/2$ ; and experimental result, the central wavelength is 1580.02 nm.

Furthermore, according to the theoretical results, the phase differences of  $\varphi_1$ ,  $\varphi_2$  and  $\varphi_3$  in Figs. 7(a)–(d) are identified as  $\pi/2$ ,  $\pi/2$ ,  $\pi/2$ ;  $\pi/2$ ,  $\pi$ ,  $\pi/2$ ; 0, 0,  $-\pi/2$  and 0, 0,  $-\pi/2$ . It is found that the phase differences of soliton pulses can be adjusted by finely rotating the waveplate in the cavity. Own to the comprehensive interactions of bound soliton pulses, the modulation spectrum of the soliton molecule is sensitive to the time separation and the phase difference, especially for the multipulse bound solitons. This theoretical investigation provides a simple method to unveil the effects of time separation and phase difference between the soliton pulses on the spectral characteristics of soliton molecules. For science research, this robust mode-locked fiber laser delivers a prevailing platform to explore the versatile soliton molecules and multifaceted nonlinear phenomena in the cavity. Thanks to adjusting the modulation depth of the roundtrip reflectivity curve by rotating the waveplate, manipulation of the versatile soliton molecules is achieved at different pump powers. All these findings have demonstrated the multifaceted nonlinear dynamics in this excellent architecture, and pave the potential applications for this robust all PM mode-locked fiber laser with good self-starting ability and well resistance to ambient perturbation.

#### 4. Conclusion

In summary, we have experimentally demonstrated soliton molecules generation in a robust all PM mode-locked fiber laser with a non-reciprocal phase bias. The mode locking operation is self-starting and possesses excellent long-term stability. Through elaborately adjusting the waveplate in the cavity, manipulation of the laser pulse from conventional soliton to soliton molecules is achieved,

and then versatile soliton molecules, including harmonic soliton pairs, tightly or loosely bound soliton quartets, and multipulse bound solitons, are precisely manipulated at different pump powers. To the best of our knowledge, this is the first-time demonstration of various soliton molecules in this excellent architecture mode-locked fiber laser. Furthermore, the theoretical investigations are implemented to verify the spectral characteristics of soliton molecules with different phase differences and different time separations, and the theoretical results are in good agreement with the experiment. We believe this robust all PM mode-locked fiber laser delivers an ideal platform for investigating the dynamics of soliton molecules operation, as well as provides a simple, effective method to manipulation of soliton molecules that can bring potential applications in designing of optical telecommunication systems with high capacity.

## Acknowledgement

The authors wish to thank the anonymous reviewers for their valuable suggestions.

---

## References

- [1] M. Pang, W. He, X. Jiang, and P. St. J. Russell, "All-optical bit storage in a fibre laser by optomechanically bound states of solitons," *Nat. Photon.*, vol. 10, pp. 454–458, 2016.
- [2] L. F. Mollenauer and K. Smith, "Demonstration of soliton transmission over more than 4000 km in fiber with loss periodically compensated by raman gain," *Opt. Lett.*, vol. 13, no. 8, pp. 675–677, 1988.
- [3] W. J. Firth and C. O. Weiss, "Cavity and feedback solitons," *Opt. Photon. N.*, vol. 13, pp. 54–58, 2002.
- [4] B. A. Malomed, "Bound solitons in the nonlinear schrödinger ginzburg-landau equation," *Phys. Rev. A*, vol. 44, no. 10, pp. 6954–6957, 1991.
- [5] D. Y. Tang, W. S. Man, H. Y. Tam, and P. D. Drummond, "Observation of bound states of solitons in a passively mode-locked fiber laser," *Phys. Rev. A*, vol. 64, pp. 033814–1–033814–3, 2001.
- [6] P. Grelu, F. Belhache, F. Gully, and J. M. Soto-Crespo, "Phase-locked soliton pairs in a stretched-pulse fiber laser-grelu2002," *Opt. Lett.*, vol. 27, no. 11, pp. 966–969, 2002.
- [7] B. Ortaç, *et al.*, "Generation of parabolic bound pulses from a Yb-fiber laser," *Opt. Exp.*, vol. 14, no. 13, pp. 6075–6083, 2006.
- [8] L. Zhao, D. Tang, X. Wu, D. Lei, and S. Wen, "Bound states of gain-guided solitons in a passively mode-locked fiber laser," *Opt. Lett.*, vol. 32, no. 21, pp. 3191–3192, 2007.
- [9] H. Qin, X. Xiao, P. Wang, and C. Yang, "Observation of soliton molecules in a spatiotemporal mode-locked multimode fiber laser," *Opt. Lett.*, vol. 43, no. 9, pp. 1982–1985, 2018.
- [10] T. Zhu, Z. Wang, D. Wang, F. Yang, and L. Li, "Observation of controllable tightly and loosely bound solitons with an all-fiber saturable absorber," *Photon. Res.*, vol. 7, no. 1, pp. 61–68, 2019.
- [11] D. Y. Tang, B. Zhao, and L. M. Zhao, "Soliton interaction in a fiber ring laser," *Phys. Rev. E*, vol. 72, pp. 016616–1–016616–10, 2005.
- [12] Y. Wang, F. Leo, J. Fatome, M. Erkintalo, S. G. Murdoch, and S. Coen, "Universal mechanism for the binding of temporal cavity solitons(optica)," *Optica*, vol. 4, no. 8, pp. 855–863, 2017.
- [13] T. Jiang, Y. Cui, P. Lu, C. Li, A. Wang, and Z. Zhang, "All PM fiber laser mode locked with a compact phase biased amplifier loop mirror," *IEEE Photon. Technol. Lett.*, vol. 28, no. 16, pp. 1786–1789, Aug. 2016.
- [14] W. Hänsel *et al.*, "All polarization-maintaining fiber laser architecture for robust femtosecond pulse generation," *Appl. Phys. B*, vol. 123, no. 41, pp. 1–6, 2017.
- [15] G. Liu, X. Jiang, A. Wang, G. Chang, F. K. Aertner, and Z. Zhang, "Robust 700 MHz mode locked yb fiber laser with a biased nonlinear amplifying loop mirror," *Opt. Exp.*, vol. 26, no. 20, pp. 26003–26009, 2018.
- [16] W. Gao, G. Liu, and Z. Zhang, "China. "44.6 fs pulses from a 257 MHz er fiber laser mode\_locked by biased NALM," *Opt. Lett.*, vol. 16, no. 11, pp. 111401–111402, 2018.
- [17] R. L. Zhou, X. Liu, G. Liu, H. Y. Fu, and Q. Li, "Robust all polarization-maintaining femtosecond fiber laser with various phase bias," in *Proc. 18th Int. Conf. Opt. Commun. Netw.*, China, Huangshan, 2019, pp. 1–3.
- [18] L. M. Zhao, D. Y. Tang, T. H. Cheng, H. Y. Tam, and C. Lu, "Bound states of dispersion-managed solitons in a fiber laser at near zero dispersion," *Appl. Opt.*, vol. 46, no. 21, pp. 4768–4773, 2007.
- [19] C. B. Mou, S. V. Sergeyev, A. G. Rozhin, and S. K. Turitsyn, "Bound state vector solitons with locked and precessing states of polarization," *Opt. Exp.*, vol. 21, no. 22, pp. 26868–26875, 2013.
- [20] D. Y. Tang, L. M. Zhao, and B. Zhao, "Multipulse bound solitons with fixed pulse separations formed by direct soliton interaction," *Appl. Phys. B*, vol. 80, pp. 239–242, 2005.
- [21] L. Gui, X. Xiao, and C. Yang, "Observation of various bound solitons in a carbon-nanotube-based erbium fiber laser," *J. Opt. Soc. Amer. B*, vol. 30, no. 1, pp. 158–164, 2003.